Combining brainwide activity imaging and electron microscopy reveals novel nociceptive circuits

Nadine Randel*[,c,1,2,3], Chen Wang*[,6], Michael S. Clayton[3], Kun Wang[3], Song Pang[5], Shan C. Xu[6], Andrew Champion[3,5], Harald F. Hess[7], Albert Cardona[c,3,2], Philipp J. Keller[c,7] and Marta Zlatic[c,3,1]

* *First co-authors*

Affiliations

1) University of Cambridge, Department of Zoology, Cambridge CB2 3EJ, United Kingdom
2) University of Cambridge, Department of Physiology, Development and Neuroscience, Cambridge CB2 3EL, United Kingdom
3) MRC Laboratory of Molecular Biology, Cambridge CB2 0QH, United Kingdom
4) Janelia Research Campus, Ashburn, VA 20147, United States
5) Janelia Research Campus, Ashburn, VA 20147; Yale School of Medicine, New Haven, CT 06511, United States
6) Janelia Research Campus, Ashburn, VA 20147; Department of Cellular and Molecular Physiology, Yale School of Medicine, New Haven, CT 06520, United States
7) Janelia Research Campus, Ashburn, VA 20147, United States

[c] *Correspondence*

Albert Cardona: acardona@mrc-lmb.cam.ac.uk
Philipp Keller: kellerp@janelia.hhmi.org
Nadine Randel: nr479@cam.ac.uk
Marta Zlatic: mzlatic@mrc-lmb.cam.ac.uk

Abstract

To understand how brains work, it is necessary to connect neural activity to synaptic-resolution circuit architecture. Recent advances in light-sheet microscopy (LSM) enable whole-brain, cellular-resolution imaging of activity of all neuronal cell bodies, however most neurons from such datasets cannot be identified. In most organisms, neurons are identifiable based on their projections (and not based on their cell body position) which cannot be resolved in using LSM. Here, we present a novel methodology to overcome this by combining *in vivo* whole-brain activity imaging, with subsequent electron microscopy imaging of the same brain to visualise neuronal projections and identify neurons with interesting activity. We used this approach to identify brain neurons involved in nociception in *Drosophila* larva. After whole-brain imaging of activity during nociceptive stimulation, we imaged the same brain with an enhanced focused ion-beam electron microscope (eFIB-SEM). We registered the functional and anatomical volumes and reconstructed (in the eFIB-SEM volume) the projections of neurons that responded to nociceptive stimulation to determine their developmental lineage and identity. This revealed a distributed nociceptive network spanning 25 distinct lineages and many distinct brain areas, and included direct brain targets of nociceptive projection neurons that integrate nociceptive information with other sensory modalities, as well as brain output neurons (descending neurons [DN]) that likely contribute to action-selection. Surprisingly, we also found neurons previously previously associated with olfaction and learning, such as Kenyon cells. Our workflow provides a powerful framework for mapping neuronal activity onto structure across an entire brain, yielding novel insights into the central processing of noxious stimuli.

Introduction

In order to behave adaptively in the environment, animals must process incoming sensory information and select appropriate actions but we still lack a comprehensive understanding of neural circuits that underlie these fundamental brain functions. One major challenge is that even seemingly simple behaviours, such as responses to innately aversive stimuli, are flexible and subserved by circuits that are not restricted to small, specific brain regions but distributed across many areas of the central nervous system.

Our understanding of neuronal mechanisms has been greatly advanced by access to whole-brain connectomes, which reveal the patterns of connections between all neurons in the brain [1–9]. However, while synaptic-resolution connectivity maps are essential for understanding how neural circuits implement fundamental brain functions, by themselves they are not sufficient. To gain a mechanistic understanding of circuit function, in addition to knowing their connectivity patterns, it is also necessary to characterise neuronal activity patterns during a range of behavioural tasks. Indeed, numerous previous studies have shown the importance of linking both synaptic connectivity and neuronal activity on a single cell level to gain a detailed mechanistic understanding of neural circuit mechanisms [10–26].

However, most studies use genetic tools to selectively label and analyse response properties of one identified neuron type at a time. By combining recordings from different neurons, populations, or regions, from many different animals during the same task, information about response properties from different neurons can slowly be accumulated. The problem with this approach is that it is very slow, and it would take a very long time to obtain information from all neuron types, during the same tasks. Furthermore, correlations in activity between different neuron types in the same individual cannot be properly assessed.

Recently, advances in light-sheet microscopy (LSM) have opened doors to imaging activity of all neurons in the entire brain of relatively small animals with single cell resolution, including nematode worms, insects, and even small vertebrates [27–30]. Such datasets can comprehensively reveal all neuronal cell bodies with specific response properties. However, in most brains larger than *C. elegans*, including those of small insects like *Drosophila* larvae, cell body position is insufficient to identify neurons. It is, therefore, impossible to combine information about activity of specific neurons from such datasets with previously available information about these neurons - such as their developmental origin (lineage), projection pattern, synaptic connectivity, or molecular properties. In contrast to cell body position, most neurons can be uniquely identified based on the shape and location of their projections. However, while light-microscopy provides sufficient resolution to resolve densely labelled cell bodies from each other (each about 5um in diameter), it does not provide sufficient resolution to resolve densely labelled neuronal projections in neuropil areas.

We have therefore developed a methodology that enables us to visualise the projections of all neurons after imaging their activity with light-sheet microscopy, in order to identify neurons based on their projections and combine this information with known information about their connectivity and other properties. Our approach involves imaging the same nervous system with electron microscopy after whole-brain imaging of neural activity. Electron microscopy (EM) can provide sufficient resolution to resolve densely labelled projections of all neurons in the nervous system, and identify neurons based on their projection patterns after segmenting large axonal and dendritic branches. Furthermore, recent advances in electron microscopy enable imaging entire brains of small animals relatively rapidly. For example, a brain of a *Drosophila* larval (100 µm x 100 µm x 80 µm) can be imaged in one go in under ten days with 8 x 8 x 8 nm/voxel resolution with a single enhanced focused ion-beam electron microscope (eFIB-SEM), and other methods allow for even faster imaging of larger brains [31–33].

We applied this approach to identify novel elements of nociceptive circuits in the brain of the tractable insect model system, the *Drosophila* larva. The *Drosophila* larva is an excellent model system for brainwide analysis of neural circuit structure and function and for elucidating the circuit mechanisms of fundamental brain functions. Larvae have a rich behavioural repertoire, the complete synaptic-resolution connectome of the *Drosophila* larval brain has recently been published and an exquisite genetic toolkit is available for selectively targeting and manipulating individual neuron types to elucidate their roles in behaviour [13,15,16,34–41].

Larval nociceptive circuits have been extensively studied and multiple neurons that respond to noxious stimuli and contribute to innate escape responses have been identified in the ventral nerve cord [13,42–45]. Interestingly, these studies, as well as the connectome, have revealed that nociceptive information is relayed to the brain via ascending projection neurons that are also activated by nociceptive stimuli and that facilitate innate escape responses [13,37]. However, the number and types of brain neurons that respond to noxious cues, their lineage identity, and whether and how they contribute to innate responses to noxious cues is unknown.

Here, we first imaged calcium transients of all neurons in the larval brain using multi-view LSM while providing targeted stimulation of the primary nociceptive interneurons in the nerve cord. Subsequently, we imaged the same brain with an eFIB-SEM (imaged at 12 x 12 x 12 nm/pixel resolution), registered the LSM and eFIB-SEM volumes of the same brain to each other, reconstructed the large projections of all neurons that had significant responses to noxious cues, to reveal their developmental origin (lineage identity), and then traced finer branches for a subset of them to uniquely identify them. We then validated our approach by using GAL4-lines to selectively express GCAMP in the identified brain neurons and confirm they respond to noxious stimuli, as revealed by pan-neuronal imaging of activity [39].

Our unbiased comprehensive approach provided novel insights into nociceptive circuits. We found ca. 4% of brain neurons responded significantly to a nociceptive stimulus, most of which were previously not known to respond to these stimuli. The newly identified neurons that respond to nociceptive stimuli spanned a range of neuron categories[37], including brain neurons that receive input from somatosensory projection neurons, brain output neurons (descending neurons [DN] that project to the suboesophageal zone [SEZ] and the ventral nerve cord [VNC]), as well as neurons presynaptic to the brain output neurons (pre-DN). Surprisingly, we also found neurons previously thought to be implicated in processing olfactory stimuli (lateral horn neurons, [LHNs]) and even intrinsic neurons of the learning circuit, mushroom body Kenyon Cells (KCs) and output neurons (MBONs) responded to nociceptive cues.

Together, this study provides novel insights into processing of nociceptive stimuli in the insect brain. The methodology developed in this study will enable overlaying activity patterns during a range of different behavioural tasks onto the connectome and provides a basis for a comprehensive brainwide understanding of neural circuit function.

Results

Methodology for overlaying brainwide activity and connectivity maps

In order to identify brain neurons with specific functional response properties in an unbiased and comprehensive way, we developed a methodology for overlaying brainwide activity and connectivity maps (Figure 1A-J).
We expressed a calcium indicator of neural activity (RGECO1a) ubiquitously, in all neurons, and the optogenetic activator of neural activity (Chronos), selectively in a subset of nociceptive interneurons in the nerve cord, called Basins, that receive direct synaptic input from nociceptive sensory neurons and whose optogenetic activation evokes a strong escape response [13,62]. We imaged the activity of every neuron in the extracted nervous system of a first instar larva with a multi-view LSM, before, during and after optogenetic activation of Basins in the fourth abdominal segment (Figure 1A, B). We presented a total of 18 nociceptive stimuli with 200 s between each stimulation.

Immediately after the functional experiment, we processed the sample for volume EM acquisition, by chemically fixing it, followed by staining using an adapted OTO protocol with lead aspartate to enhance contrast [63]. We then imaged the entire CNS with eFIB-SEM at 12 x 12 x 12 nm resolution. This resolution is lower than the 8 x 8 x 8 nm resolution used to image adult fly brains, but we reasoned it could be enough to allow tracing of major neuronal branches (even if not finer branches and synapses) [64]. After acquiring the eFIB-SEM volume, we registered the datasets of the two imaging modalities, using 51 landmarks detectable in both volumes (Figure 1D, E, 2A). Based on this registration, the segmented nuclei in the EM volume were projected into the LM volume to extract their changes in fluorescence at single cell resolution (Figure 2B). Consequently, we were able to locate nuclei in the EM volume whose activity correlated with the optogenetic manipulation of Basin neurons.

From the ~3000 brain neurons, 119 neurons (~4%) responded consistently and significantly to the activation of Basin neurons. To identify the developmental origin (lineage) of these neurons we manually reconstructed their large neuronal arbours up to their entry point into the neuropil and a little beyond (Figure 1C, 2C). Based on their entry point into the neuropil, we identified 25 cell lineages that each contained between 1-20 neurons that responded to nociceptive stimulation (Figure 2).

Next, we randomly selected 50 neurons to determine what fraction of them can be uniquely identified from our 12 x 12 12 nm resolution FIB-EM dataset. For this purpose, we traced their fine branches as far as possible and then compared the shapes of their projections to the shape of the reference neurons from our recently published complete reconstructions of all neurons in a larval brain (and their synaptic connections [37]). We were able to trace 26/50 neurons, whereas the remaining 24 were not traceable due to imaging artifacts in the EM volume. We were able to uniquely identify 18/26 unique neurons and 8/26 neurons with two to four candidates within the same lineage due to their high morphological similarity (Figure 1F, 3E,F,H,L,N).

Finally, to validate our methodology, we searched for available GAL4 lines that selectively target gene expression to these neurons [39]. We were able to identify lines for only 3 out of the 26 neurons. We used these GAL4 lines to selectively express GCAMP6 in each of these

neurons, and imaged their responses to Basin activation using two-photon microscopy [49]. We confirmed that they all had similar responses when imaged individually, to the responses obtained using whole-brain imaging, thereby validating our ability to correctly identify neurons after whole-brain imaging of neural activity (Figure 1G, H).

Identifying brain neuronal lineages activated by noxious stimuli

The *Drosophila* larval brain contains approximately 100 stereotyped neuronal lineages. Neurons from each lineage derive from a single neuroblast and follow a characteristic trajectory to the neuropil and enter the neuropil at a stereotypic location and project into similar neuropil areas [65]. The lineage identity of each neuron can therefore be uniquely identified based on the trajectory its axon takes to the neuropil and the neuropil entry point.

To identify the lineage of each of the 119 neurons that significantly responded to Basin activation, we therefore manually traced their axons that lead from the cell body to the neuropil entry point and beyond (Figure 2). We were able to trace 102/119 neurons (86%), and the remainder could not be traced due to image artifacts in the EM volume. Based on their neuropil entry point, we identified 25 neuronal lineages that each contained between 1-30 neurons that responded to nociceptive stimulation (Figure 2, Table 1).

We wondered whether neurons from lineages that received the most direct Basin input were more likely to respond to Basin activation, than others. Therefore, we analysed the published connectome of *Drosophila* larval brain ([37]) and found that 82 lineages contain neurons that receive Basin input within ≤5 hops. 25 of these 82 lineages contained neurons that significantly responded to Basin activation in our whole-brain imaging experiments. None of the neurons from lineages that contained neurons that were not connected to Basins with 5 or less hops responded to Basin activation. Interestingly, only 15 lineages contained neurons that received two-hop input from Basins (via direct input from ascending projection neurons from the nerve cord that in turn receive direct Basin input), but 10 out of these contained neurons that significantly responded to Basin activation (Figure 2E–Z; Table 1). Thus, 40% of the 25 lineages whose neurons responded to Basins received one-hop input from Basins. Overall our data reveal that neurons from lineages that contain the most direct, two-hop, input from Basins are more likely to respond to Basin activation, than neurons from lineages that receive more indirect input via longer paths: 10/15 (67%) vs. 15/67 (22%).

Next we analysed the activity of the neurons within the same lineage. We discovered that all neurons within a single lineage responded similarly to the stimulus. The activity traces often overlapped, and all neurons were either depolarised or hyperpolarised upon Basin activation. The only exception was the cell lineage BLAv1/2, where 2 out of 30 depolarised cells responded via hyperpolarisation (Figure 2G). The results indicate that the neurons within a lineage mainly respond in a similar fashion, either being depolarised, or hyperpolarised.

Identifying individual brain neurons activated by noxious stimuli

Next, we randomly selected 50 neurons that significantly responded to Basin activation to determine what fraction of them we can identify as homologous to one of the neurons from the reference brain. We traced their fine projections and compared their morphology to the

reference neurons from our recently published reconstructions of all larval brain neurons [37]. In our 12 x 12 x 12 nm/pixel resolution eFIB-SEM dataset, of the selected neurons, we were able to trace 18 sufficiently to identify them (MB2IN-172, CSD, MB2IN-196 UT, BLAv1/2 ring like left and right, Basal-Tel-like 6, MBON-q1, PVC, BLVp1 bilateral, BLVp12 desc left and right, CM13 bilateral 3, CM13 desc and 5 Kenyon cells [KCs]); 8 could be narrowed down to 2-4 candidates with very similar projections belonging to the same neuron types within the same lineage (BALp desc 1 or 3; Basal Tel-like 2 or 5; Switcheroo 1, 2, 3, or 4; two Lasso-top neurons that could each be one Lasso-top 1 - 3; and 3 neurons that each could be BLAv12 ipsi 1 or 2, or BLAv12_ant desc 1 [Figure 3A-T and Table 2]) and the remainder could not be traced sufficiently to allow identification. 20/26 identified neurons were depolarised and 6/26 hyperpolarised in response to Basin activation (Figure 3A-T and Figure 4A-O).

All identified cells, except Lasso-top, received input from Basins via two to five hops, some forming strong hubs within the network, such as Basal Tel-like 2, 5, Basal Tel-like 6, BALv12-ring-like, and CM13 descending (Figure 5). These neurons integrate information from multiple other neurons of the nociceptive circuit. We also discovered recurrent feedback connections onto Basins from two of the hub neurons, MB2IN-196 UT and MB2IN-172.

We analysed in more detail the 26 identified neurons (Table 2). Three identified brain neurons receive the shortest possible, two-hop, input from Basins, via direct synaptic input from ascending projection neurons (A00c) that receive direct Basin input: Basal-Tel-like 2, 5, Basal-Tel-like 6, and BLAv12 ipsi 1 (Figure 5). Basal Tel-like 2, 5 and Basal Tel-like 6 integrate nociceptive information from the two sides of the body. Basal Tel-like 2,5 also receives direct input from other somatosensory ascending projection neurons. These neurons also integrate nociceptive input with other sensory modalities via input from LHNs.

Furthermore, Basal Tel-like 2, 5 and Basal Tel-like 6 directly innervate brain output neurons (DNs), thus participating in short nerve cord-brain loops. Thus, they both directly innervate the DN-SEZ neuron BLAv1/2 ring, and Basal Tel-like 2, 5 also directly innervates the DN-VNC BLVp12 desc.

One third of the identified neurons were DNs (19% DN-VNC and 12% DN-SEG), transmitting the signal from the brain to the VNC, or to SEZ. This includes five DN-VNC neurons (CM13 desc, BAlp desc 1 or BAlp desc 3, Switcheroo 1-4, BLVp12 desc left and right), and three DN-SEZ (MB2IN-172, BLAv1/2 ring like left and right). Four neurons were directly upstream of DNs (pre-DN-VNCs [CM13 bilateral 3, CSD, BLAv12 ipsi 2, and BLAv12 ant desc 1]. Four neurons did not belong to any previously described neuron categories (Lasso-top 1-3 neurons, BLVp1 bilat, PVC).

Surprisingly, we also found neurons previously implicated in processing olfactory stimuli (a lateral horn neuron, [LHNs], MB2IN-196 UT) and even five Kenyon Cell (KCs), the intrinsic neurons of the learning circuit, the mushroom body (MB), and an MB output neuron (MBON-q1) responded to nociceptive cues [35,4138,66]. Interestingly, KCs are probably one of the most studied neurons in the *Drosophila* nervous system, but despite this, they were never previously reported to respond to noxious cues, as they are usually thought of as representing conditioned stimuli (odours, temperature, light), but not unconditioned ones (e.g. rewards and punishments).

Together, these findings expand our knowledge of nociceptive processing in the insect brain and provide a slew of candidate neurons for future follow-up studies.

Validating identified brain neurons

Finally, we wanted to validate our entire methodology and ability to correctly identify neurons after whole-brain imaging of neural activity, followed by eFIB-SEM imaging, registration and tracing of neuronal projections in the eFIB-SEM volume. To do this, we looked for available GAL4 lines that drive expression selectively in the neurons that we identified as responding to Basin activation. We were able to find GAL4 lines for 2/26 of the identified neurons: MB2IN-172 and CSD, as well as a line that drives expression in all KCs [66,67].

We then used these GAL4 lines to express GCAMP6, selectively in the neurons of interest, and the Basin-LexA to express the optogenetic activator of neural activity, Chrimson, selectively in Basin neurons. We optogenetically activated Basins and imaged the responses of KCs; MB2IN-172 or CSD using two-photon microscopy (Figure 4A-O). The results reproduced our findings from the whole brain imaging experiment, where Kenyon cells and MB2IN-172 were depolarised, and CSD was hyperpolarised upon Basin activation (Figure 3C,D,O and Figure 4F,K,O).

Overall, these experiments validate our methodology and ability to identify neurons after whole-brain imaging of neural activity.

Discussion

In this study we developed a novel methodology for identifying neuron types and individual neurons, after following cellular-resolution whole-brain imaging with LSM. While cell body position alone is not sufficient to identify neurons, most neuron types (and even individual neurons) can be identified based on the locations and shapes of their projections. Our methodology, therefore, involves imaging the same brain with higher-resolution EM, to visualise neuronal projections, followed by reconstruction of the branches of those neurons that have interesting activity properties. This approach enables combining information about neuronal activity with previously available information about each neuron, such as their synaptic connectivity, molecular properties, or roles in behaviour.

We applied our approach to gain a better understanding of the processing of nociceptive stimuli in the brain of *Drosophila* larvae. After pan-neuronal calcium imaging in response to optogenetic activation of nociceptive interneurons (Basins), we imaged the same CNS with eFIB-SEM at 12 x 12 x 12 nm/pixel resolution, sufficient to visualise medium-sized neuronal branches (but not fine ones), and registered the two datasets of the same brain to each other, using landmark-based registration. From the LSM dataset we found that 119 neurons significantly responded to Basin activation. We randomly selected 50 of these neurons for follow up and manually traced their medium-sized branches in the eFIB-SEM volume. Because automated segmentation algorithms were all trained on 8 x 8 x 8 nm resolution datasets in *Drosophila*, for this proof-of-principle study, we manually traced neuron arbours and were therefore not able to follow-up all the neurons. 26/50 could be traced sufficiently to identify them, either uniquely, or to a neuron type with very similar projections within the same lineage. Finally, we validated our neuron identification using GAL4 lines to selectively

drive GCAMP in some of the identified neurons and confirming they reproducibly respond to optogenetic activation of nociceptive interneurons in multiple individuals.

Prior studies show that imaging *Drosophila* brains with eFIB-SEM using 8 x 8 x 8 nm/pixel resolution is sufficient to reconstruct neuronal fine branches and synapses [9,64]. Here we chose a lower, 12 x 12 x 12 nm/pixel resolution, to assess the extent to which medium-sized branches will be traceable and the extent to which this would be sufficient for identifying neurons. While, for *Drosophila* larval brains, imaging with 8 x 8 x 8 nm resolution would be very fast (ten days per brain), imaging with 12 x 12 x 12 nm resolution is 30% faster, and would enable acquisition of large sample sizes, or faster imaging of larger brains. Overall, our study demonstrated that, after cellular-resolution imaging with LSM, imaging the same brain with 12 x 12 x 12 nm/pixel eFIB-SEM, enables identification of ca. 50% of neurons. In the future, for smaller brains, such as that of *Drosophila* larva, imaging with synaptic-resolution (8 x 8 x 8 nm/pixel) would be fast enough and would provide significant advantages: first, it would enable tracing of fine branches and synapses; second, it would enable automated segmentation of neuronal branches using existing models and therefore identification of most neurons in the brain [64]. As EM imaging and reconstruction gets faster and faster, it may be possible to apply this approach to larger and larger brains [31–33,68]. Furthermore, expansion microscopy may also be used instead of EM to visualise neuronal projections following whole-brain imaging of neural activity [69–72].

Nociceptive circuits in the *Drosophila* larval nerve cord have been extensively studied, but much less was known about nociceptive signalling in the brain. Here we discovered multiple novel neuron types responsive to nociceptive stimuli. 20/26 (77%) of identified neurons were depolarized and 6/26 (23%) hyperpolarized in response to nociceptive neuron activation. We discovered hub-neurons for nociceptive processing, as well as feedback neurons that signal back to the first-order nociceptive interneurons (Basins), likely modulating their response to pain. Identified neurons also included direct targets of nociceptive ascending projection neurons in the brain, some of which integrate nociceptive information from two sides of the body, while others integrate nociceptive information with other sensory modalities, as well as brain descending neurons that project to the premotor regions of the nerve cord and could play a role in facilitating responses to nociceptive stimuli. Surprisingly, we also discovered nociceptive responses in neuron types and brain areas previously associated with olfactory processing. For example, a subset of MB Kenyon Cells, the intrinsic neurons of the learning circuit, responded to nociceptive interneuron activation. KCs are essential for associative learning, and have been demonstrated to encode conditioned stimuli (CS), such as odours, light, or temperature that can be associated with unconditioned stimuli, US, such as noxious stimuli [73–77]. Surprisingly, our study shows that a subset of KCs responds to nociceptive stimulation. Indeed, analysing the connectome reveals axo-dendritic paths from Basin neurons to a subset of KCs. Thus, the MB could influence innate decision-making in response to nociceptive cues, or it could play a role in learning to respond more or less strongly to noxious stimuli based on previous experience.

These findings demonstrate how unbiased, whole-brain imaging approaches can reveal unexpected response properties, even for one of the most studied cell types in the insect brain. Furthermore, for many of the identified neurons, GAL4 lines are not available, underscoring the importance of whole-brain imaging to study the response properties of a large fraction of neurons for which genetic driver lines are not available.

In summary, our study identified multiple neuron types in the insect brain involved in processing nociceptive stimuli. The methodology we have developed will enable overlaying brainwide activity maps during various behavioral tasks onto connectivity maps, an essential step towards understanding neural circuit function.

Acknowledgements

The authors thank MRC Laboratory of Molecular Biology, HHMI Janelia Research Campus and Department of Zoology, University of Cambridge for funding and support; Bill Lemon (HHMI Janelia Research Campus), Fly core (especially Monti Mercer) at JRC, and Nan Hu and Oxana Elliott at the Department of Zoology, University of Cambridge for fly crosses; Will Bishop for extremely useful discussions and feedback; the Janelia Visitor Project for outstanding support over the years; MRC Laboratory of Molecular Biology Core funding (MZ, AC, MJW and KW), HHMI Janelia Research Campus (MZ, AC, PJK, NR, CW, HFH, SCX, SP), Wellcome Trust grant 205038/Z/16/Z (AC), Wellcome Trust grant 205050/Z/16/Z (MZ), ERC grant ERC-2018-COG: 819650 (MZ, NR) for funding.

Material and methods

Fly lines

Whole-brain calcium imaging

Flies expressed UAS-RGECO1a pan-neuronally for monitoring neuronal activity, and LexAop-Chronos in the primary nociceptive interneurons, Basins (72F11-LexAp65), for optogenetic activation [13,46–48].

The final cross LexAop-Chronos (attP18)/ +/Y; 72F11-LexA (JK22)/ UAS-H2B-GFP (attP5); UAS-RGECO1a (VK0005)/ 57C10-GAL4 (attP2) was made by using the following stocks: 13XLexAop2 IVS p10 Chronos mVenus (attP18), 72F11-LexAp65 (JK22C), and 20XUAS-IVS-NES-jRGECO1a-p10 (VK00005) from public collection at HHMI Janelia Research Campus (Ashburn, VA, US); 20XUAS-H2B-GFP-p10 in su(Hw)attP5 gift from Wilhelm Lemon - Philipp Keller lab, HHMI Janelia Research Campus (Ashburn, VA, US); and 57C10-GAL4 (attP2) from Marta Zlatic lab - MRC LMB (Cambridge, UK) [13,39,48].

Two-photon imaging

Neuronal activity was recorded from specific cells expressing GCaMP6s during optogenetic activation of Basins that express CsChrimson [47,49].
Crosses were made using the following stocks: 72F11-LexAp65 in JK22C; 20xUAS-IV-GCAMP6s 15.641 in attp2, 13XLexop2-CsChrimson-tdTomato in VK00005 crossed with the GAL4 for MB2IN-172 and MB2IN-182, and the 14H06-GAL4 line w;14H06-LexAp65 in JK22C;13XLexAop2-IVS-GCaMP6s-p10 50.641 in VK00005,20XUAS-CsChrimson-mCherry-trafficked in su(Hw)attP1 with 72F11-GAL4 in attp2 [39,48].

Light-sheet microscopy

Sample preparation

Flies were raised on standard fly food. For the experiments, eggs were incubated at 25ºC on standard fly food with 0.5 mmol/l retinal. First instar larvae were dissected in physiological saline solution [50], and embedded in 1% low-melting temperature agarose (Sigma Aldrich Low melting agarose TYPE VII-A , Sigma (A0701)) in the physiological saline solution, as described in [51].

Data acquisition and processing

The sample was imaged using a two-view (SiMView) light-sheet microscope at HHMI Janelia Research Campus [28,52]. Imaging was performed at 2.87 Hz with a sampling resolution of 0.406 × 0.406 × 1.7 µm per pixel. A 561 nm laser was used for whole-brain imaging, while a 488 nm laser was used for optogenetic activation of Basin neurons with a dichroic mirror.
The optogenetic activation alternated between 2 s and 5 s of optogenetic stimulation with a 200 s break between each stimulation (n = 18). The resulting datasets were processed using a custom analysis pipeline as previously described [28,53].

Electron microscopy sample preparation and imaging

After functional imaging, the sample was immediately prepared for electron microscopy (EM) volume acquisition (sample ID: 1099). It was fixed in 4% glutaraldehyde in 0.1 M sodium cacodylate buffer (pH 7.4) for 1h at 4ºC, and left in the agarose cylinder during the whole preparation. All washing steps were carried out with 0.1 M sodium cacodylate buffer, until the thiocarbohydrazide step, when water was used.

Post-fixation was performed with 1.25% potassium hexacyanoferrate (II) trihydrate, 1% OsO_4 in 0.1 M sodium cacodylate buffer for 30 min at 4ºC. Next, the sample was incubated for 10 minutes in 1% filtered thiocarbohydrazide in water at room temperature, followed by 1% uranyl acetate in water overnight at 4ºC. Afterwards, the sample was incubated in pre-warmed Walton's lead aspartate for 1 h at 60ºC [54]. Finally, the sample was incubated in 0.8% OsO_4 for 30 min on ice. Following that step, the sample was dehydrated in acetone and embedded in Durcupan resin (EMS14040). The Durcupan block was finally mounted on customised soft-copper studs, which are required for the modified eFIB-SEM pipeline [55]. After trimming and coating with 10 nm gold and 100 nm carbon, the whole sample was imaged at 12 x 12 x 12 nm/px.

Landmark-based registration of EM and LM volume

To translate points between EM and LSM coordinate spaces, we identified 51 shared landmarks in the brain lobes using BigWarp [56]. The landmarks were selected, according to cell morphology and arrangement based on the moving and fixed points from the EM and LSM spaces, respectively, we calculated a thin-plate spline transformation (TPS) using the Thin Plate Spline Python library (https://github.com/raphaelreme/tps) with zero regularization ($\alpha = 0.0$).

Soma segmentation

Somas in the EM volume were segmented using a convolutional neural network (Stardist) [57], trained using a manually annotated dataset of raw images and soma segmentation masks. This process identified 11,596 putative cells across the imaged sample. The centroid of each EM soma was then determined using scikit-image functions [58], and projected into the light-sheet volume using the previously described TPS transformation. The LSM-projected centroids were then used to generate soma segmentations in the light-sheet volume. To do

this, a 3μm^3 sphere mask (corresponding to the average soma size in larval *Drosophila*) was defined and positioned at the central location of every soma. Once applied to every cell, this process generated an instance segmentation of every soma in the LSM volume, based on the initial EM segmentation.

Extraction of neuronal activity

To extract the calcium fluorescence for each soma, the LSM data was first spatially filtered to reduce low-spatial frequencies in each volume, and therefore reduce signal blur between neighbouring cells. To do this, unsharp masking was applied to each LSM volume in time using the unsharp_mask function in scikit-image (radius=5.0, amount=6.0). For each cell, the mean calcium fluorescence was extracted by calculating the mean intensity across all voxels belonging to the cell for each point in time. This generated a time-series of spatially-filtered fluorescence values for each cell. Further analyses focused only on somas in the brain and supraesophageal zone (SEZ). To do this, a bounding box was drawn around these regions and all somas positioned outside of this box were excluded (i.e. those belonging to cells in the nerve cord). This process resulted in a total of 3,480 remaining neurons.

To study soma calcium responses to Basin stimulation, we calculated stimulus-evoked calcium traces for every cell. For each stimulus delivery (n=18), fluorescence values were taken from ~5 s before and ~5 s after stimulus onset (pre-window=15 frames; post-window=15 frames; imaging frequency=2.87 Hz). For every cell, stimulus-evoked fluorescence values were normalised to the pre-stimulus baseline using the following equation:

$$\frac{\Delta F}{F_0} = \frac{F_{\text{stimulus}} - F_0}{F_0}$$

$F_{stimulus}$ is the mean fluorescence value during stimulus delivery, while F_0 is the mean calcium signal during the ~5 s before stimulus delivery. For every cell and stimulus delivery, the average fluorescence throughout the stimulus-delivery period was calculated (called 'stimulus responses' from here on).

Statistics

The reliability of cell responses to Basin stimulations were assessed by performing a one-samples t-tests on the distribution of stimulus responses for each cell, assessing whether the sample mean differed significantly from 0. Given the large number of neurons, and therefore statistical tests, p-values were corrected for false discovery rate using the Benjamini–Hochberg (negative) procedure [59] (alpha = 0.1; implemented in the Python package, statsmodels.stats.multitest.multipletests (https://www.statsmodels.org/dev/generated/statsmodels.stats.multitest.multipletests.html)). A total of 119 cells had p-values lower than the adjusted significance threshold, and were therefore identified as responding neurons to be brought forward for further analyses.

Neuron identification

Somas showing statistically significant responses to stimulation were located in the electron microscopy volume of the sample brain. The axons of selected somas were manually reconstructed using CATMAID [60]. To identify the cells, neurons of the same lineage were

reconstructed until lineage identity could be established. By comparing lineages and neurons across the sample and reference brain, cell lineage and single-cell identity was determined.

Reconstruction of neurons in eFIB-SEM volume

Neurons in the registered 12 x 12 x 12 nm/pixel resolution eFIB-SEM volume were manually reconstructed using CATMAID, as previously described [60,61]).

Synaptic connectivity and circuit analysis of identified neurons

Once neurons were reconstructed in the eFIB-SEM volume and identified based on their morphological similarity to neurons in the previously published reference volume [61]), the synaptic connectivity and circuitry of identified neurons was analysed in the reference volume, using pymaid with axon-dendritic connections (threshold: 0.01), as previously described [61].

Neuron validation

Larval Dissection and Mounting

Central nervous systems (CNSs) of third instar *Drosophila* larvae were dissected in cold saline composed of 103 mM NaCl, 3 mM KCl, 5 mM TES, 26 mM $NaHCO_3$, 1 mM NaH_2PO_4, 8 mM trehalose, 10 mM glucose, 2 mM $CaCl_2$, and 4 mM $MgCl_2$, with an osmolarity of 285 mOsm/L and pH ~7.2. Dissected brains were mounted onto a small piece of cover glass coated with poly-L-lysine (P1524; Sigma) and placed in a 35 mm petri dish lid (Falcon Easy Grip Style; Code: 351008; Scientific Laboratory Supplies), with the brain hemispheres facing upwards.

Two-Photon Imaging and Optogenetic Stimulation

A mode-locked Ti:Sapphire femtosecond pulsed laser (Spectra-Physics), tuned to 920 nm, was used for GCaMP6s imaging. Fluorescence was detected with two photomultiplier tubes (Hamamatsu) following band-pass filtering. Larval brains were imaged at 44 frames per second (fps) in a single focal plane using a two-photon microscope equipped with a fast resonant/galvo scan module (Bergamo, Thorlabs), controlled via ScanImage 2022 (http://www.scanimage.org).

Optogenetic stimulation was delivered via a high-power red LED (4-Wavelength High-Power LED Source; Thorlabs), illuminating the targeted neurons through the main optical path of the Bergamo microscope and a 25× water immersion objective (NA 1.1, WD 2 mm; Nikon). Light stimuli were delivered for 10 s (CSD), 3 s (MB2IN-172), and 5 s (Kenyon cells) with an interstimulus interval of 20 s (CSD), 27 s (MB2IN-172), and 15 s (Kenyon cells). Each trial consisted of four stimulations, automatically triggered by ScanImage 2022.

Image Analysis

Image time series were processed in Fiji (https://imagej.net/software/fiji/) and further analysed using custom scripts in MATLAB R2022a (The MathWorks, Inc). Regions of interest (ROIs) were manually defined based on the standard deviation projection of the entire time series. A background ROI was also selected outside the target cell region in each dataset to control for LED light bleed-through into the PMT for the green channel. Fluorescence signals in target ROIs were corrected by subtracting this background signal.

Fluorescence changes ($\Delta F/F_0$) were calculated as $\Delta F/F_0 = (F\cdot - F_0)/F_0$, where F_0 is the mean fluorescence over a 2-second period preceding the onset of stimulation, and $F\cdot$ is the mean fluorescence of the ROI at time t. For each brain, mean $\Delta F/F_0$ was computed across the four consecutive stimulations and averaged over three trials.

Statistical Analysis

Differences in mean fluorescent signals ($\Delta F/F$) between 7 s before and during the optogenetic stimulation were analyzed using a paired-sample t-test. A two-tailed α level of 0.05 was applied. All analyses were conducted in MATLAB R2022a.

Figures

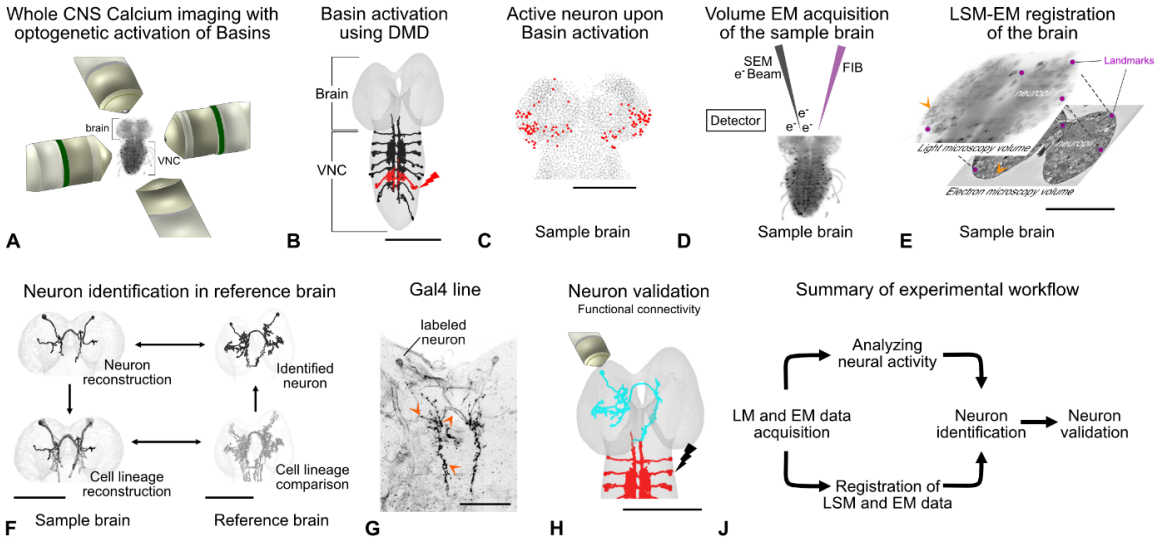

Figure 1: Overlaying single-neuron activity with synaptic connectivity. A: Whole central nervous system functional imaging with selective optogenetic activation, using multi-view light-sheet microscopy. **B:** Optogenetic activation of Basins in the fourth abdominal segment using a DMD. **C:** Brain neurons (red) that respond to Basin stimulation. **D:** Volume electron microscopy acquisition of the sample with known neuronal activity from panel A. **E:** Landmark-based registration of light and electron microscopy volumes of the same sample. **F:** Workflow of neuron identification in the sample brain, using the whole-brain reference connectome [37]. **G:** Genetic driver line of the identified neuron. **H:** Validation of identified neurons using single-neuron 2-photon imaging of single neurons with optogenetic activation of Basins. **J:** Workflow to integrate and validate single-cell neuronal activity with synaptic connectivity. Scale bar: 50 µm.

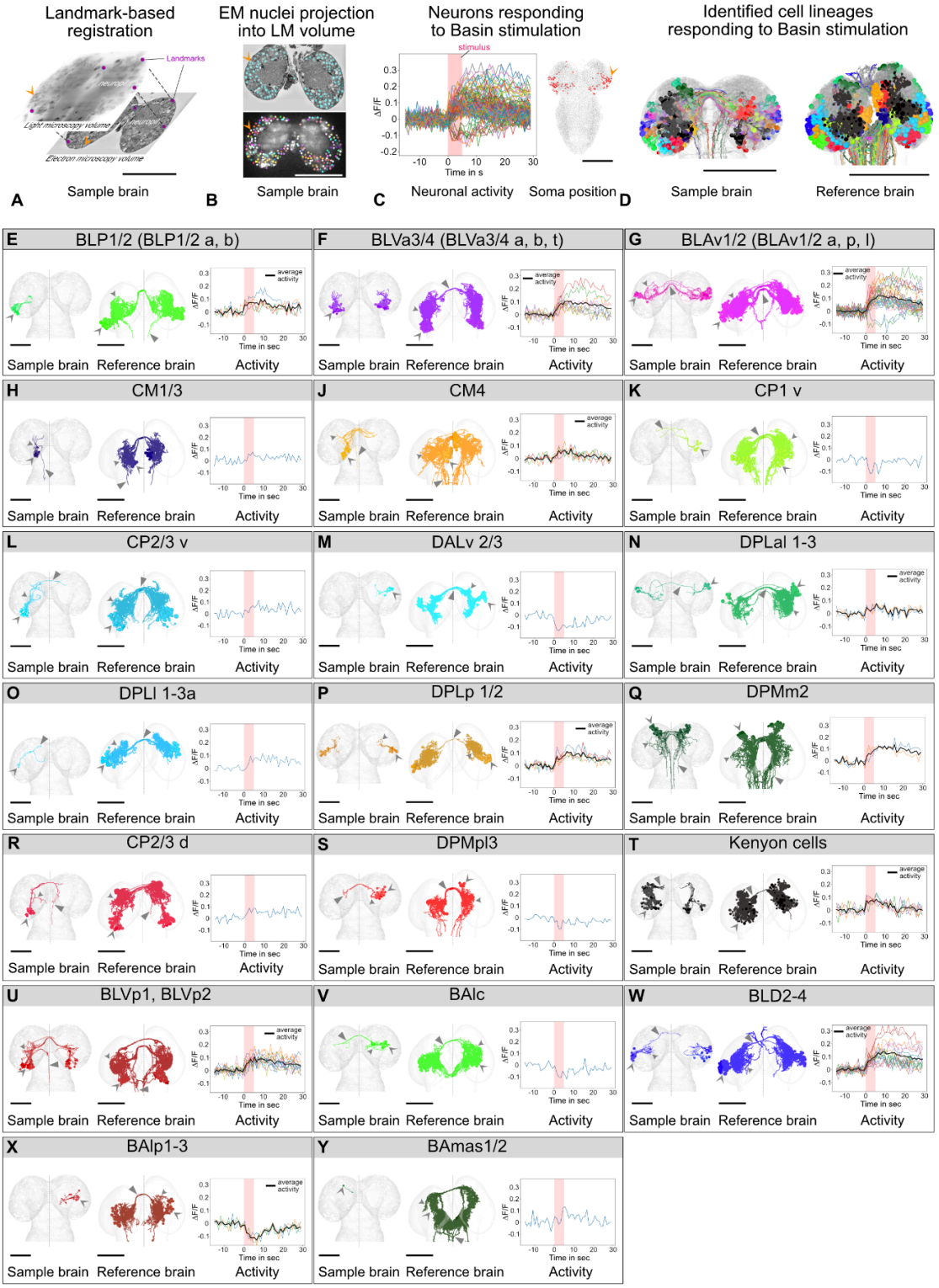

Figure 2: Cell-lineages responding to Basin activation. A: Landmark-based registration of light and electron microscopy volumes of the same sample. **B:** Automatic nuclei segmentation in the electron microscopy volume, followed by projection into the registered light microscopy volume. **C:** Activity traces and brain neuron locations that respond to Basin activation. **D:** Cell lineages responding to Basin stimulation in the sample brain and reference brain. Non-responding lineages are shown in grey. **E-Z:** Individual cell-lineages shown in both the sample and reference brain, with corresponding neuronal activity. Average traces shown in black. **G:** Hyperpolarised neurons are shown in a lighter shade. Scale bar: 25 µm. Dashed line indicates the midline, arrowheads show cell body, axon and dendrite.

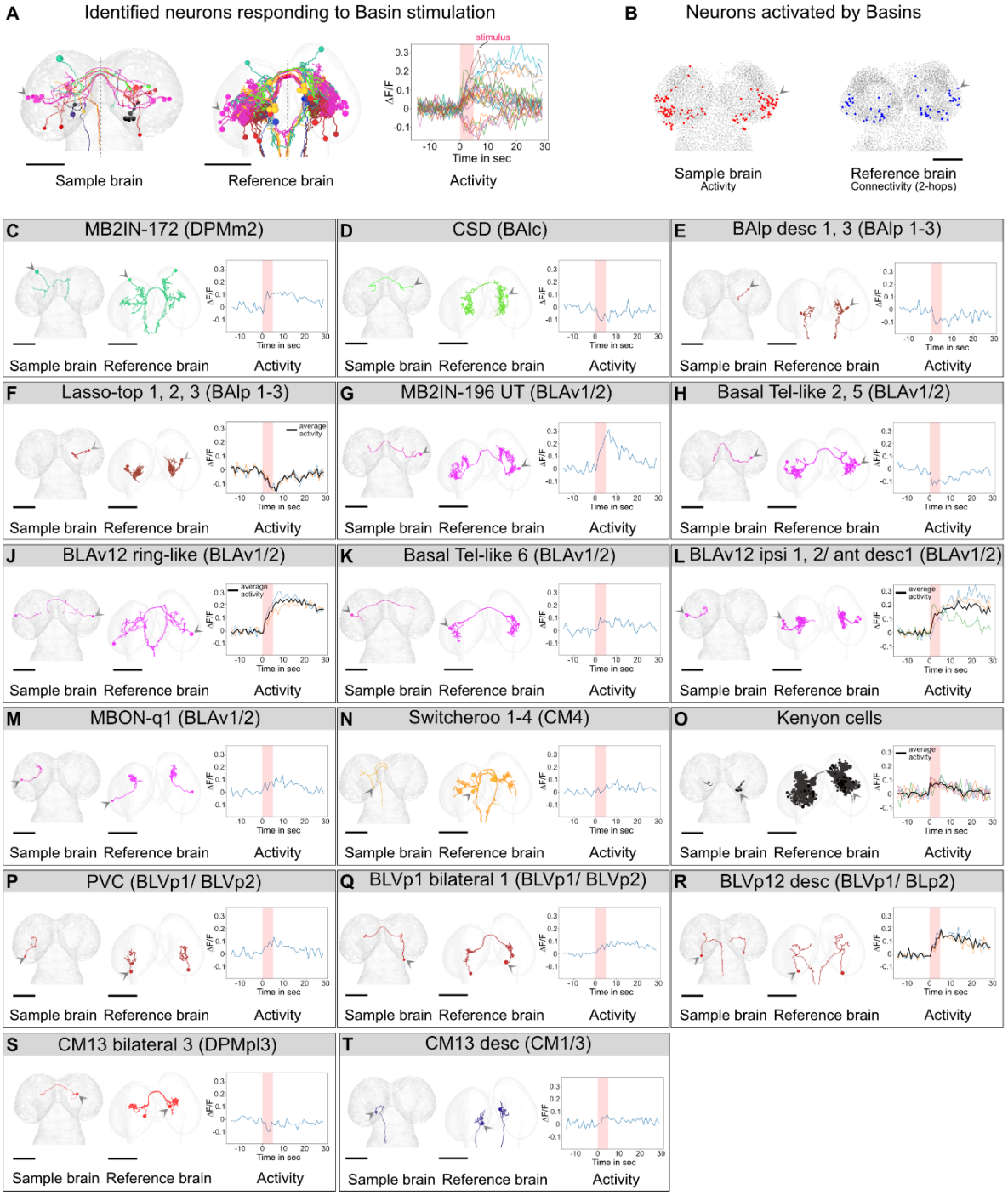

Figure 3: Identified neurons responding to Basin activation. A: Summary of identified neurons in the sample brain and reference brain, with corresponding neuronal activity. **B:** Neurons responding to Basin activation in the sample brain, and their 2-hop downstream partners in the reference connectome. **C-S:** Individual identified neurons shown in both the sample and reference brains, with corresponding neuronal activity. **E,F,H,L,N:** Candidate neurons. Individual identification was not possible due to high neuronal similarity or incomplete reconstruction. Average activity traces shown in black. Scale bar: 25 µm.

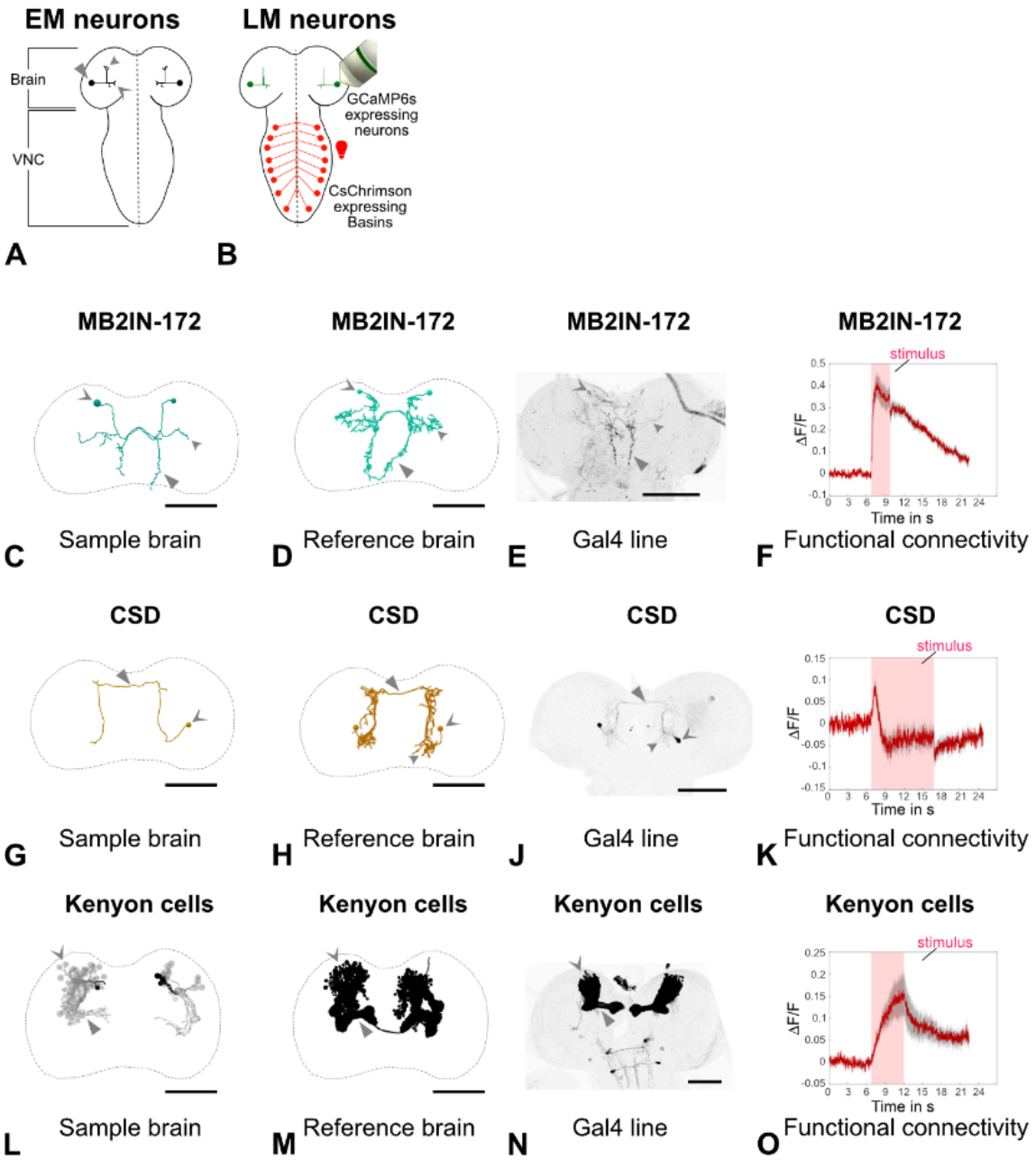

Figure 4: Neuron validation. A: Schematic of identified brain neurons. **B:** Corresponding driver line expressing GCaMP6s (left), and single neuron imaging in response to Basin activation (right). **C, G, L:** Reconstructed neurons in the sample brain. In **L**, the identified Kenyon cells are in black, and additional Kenyon cells are shown in grey. **D, H, M:** Corresponding neurons in the reference connectome. **E, J, N:** Matching driver lines expressing GCaMP6s. **F, K, O:** Neuronal responses to Basin activation recorded via 2-photon microscopy. Scale bar: **C, D, G, H, L, M**: 25 µm; **E, J, N**: 100 µm. Dashed line indicates the midline, arrowheads show cell body, axon and dendrite.

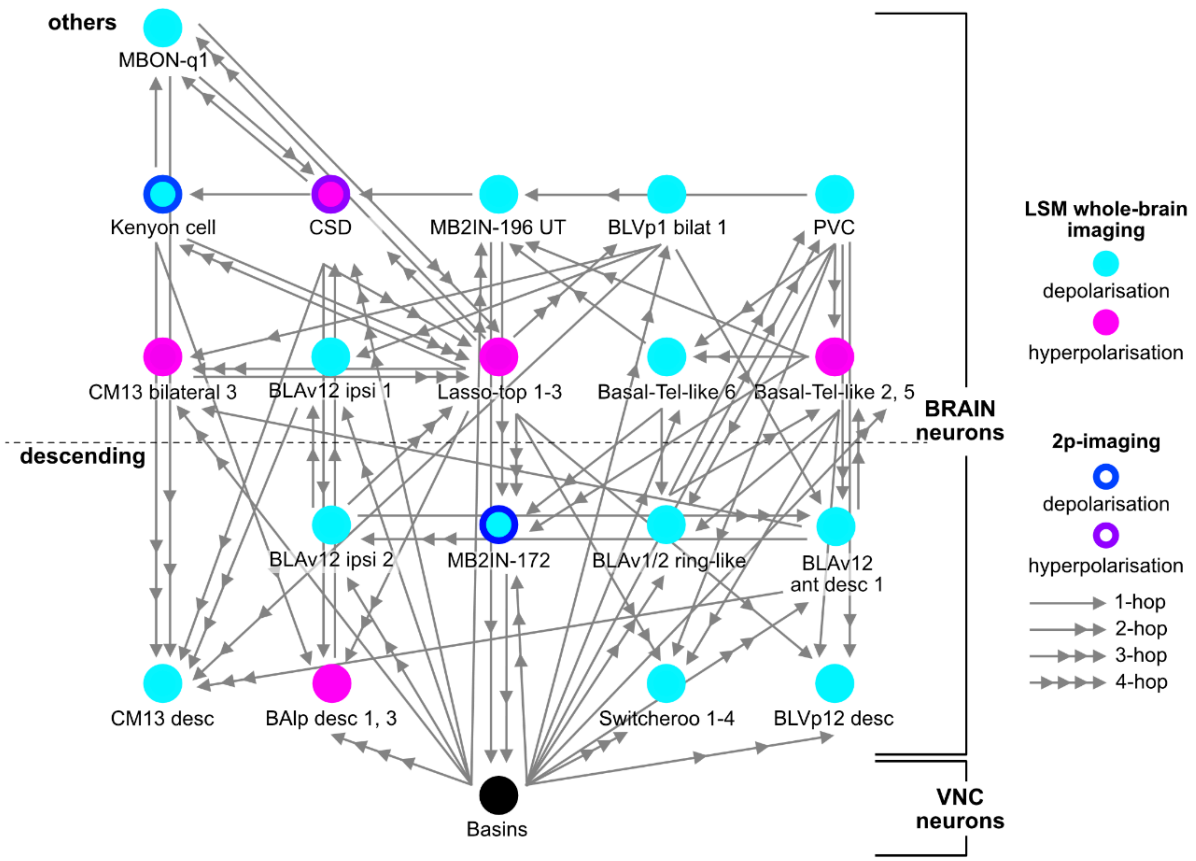

Figure 5: Neuronal connectivity of identified neurons. Shortest axon-dendritic connections for all identified neurons within ≤4hops downstream of Basins (synaptic threshold: 0.01). The number of arrowheads indicates the number of hops. Depolarised neurons are shown in cyan/blue, and hyperpolarising neurons are shown in magenta/violet.

References

1. White, J. G., Southgate, E., Thomson, J. N. & Brenner, S. The structure of the nervous system of the nematode Caenorhabditis elegans. *Philos. Trans. R. Soc. Lond. B Biol. Sci.* **314**, 1–340 (1986).
2. Verasztó, C., Jasek, S., Gühmann, M., Shahidi, R. & Ueda, N. Whole-animal connectome and cell-type complement of the three-segmented Platynereis dumerilii larva. *bioRxiv* (2020).
3. Ryan, K., Lu, Z. & Meinertzhagen, I. A. The CNS connectome of a tadpole larva of Ciona intestinalis (L.) highlights sidedness in the brain of a chordate sibling. *Elife* **5**, (2016).
4. Winding, M. *et al.* The connectome of an insect brain. *Science* **379**, eadd9330 (2023).
5. Dorkenwald, S. *et al.* Neuronal wiring diagram of an adult brain. *Nature* **634**, 124–138 (2024).
6. Witvliet, D. *et al.* Connectomes across development reveal principles of brain maturation. *Nature* **596**, 257–261 (2021).
7. Zheng, Z. *et al.* A Complete Electron Microscopy Volume of the Brain of Adult Drosophila melanogaster. *Cell* **174**, 730–743.e22 (2018).
8. Azevedo, A. *et al.* Connectomic reconstruction of a female Drosophila ventral nerve cord. *Nature* **631**, 360–368 (2024).
9. Takemura, S.-Y. *et al.* A connectome of the male*Drosophila*ventral nerve cord. *bioRxiv* (2023) doi:10.1101/2023.06.05.543757.
10. Jokura, K. *et al.* Nitric oxide feedback to ciliary photoreceptor cells gates a UV avoidance circuit. (2023) doi:10.7554/elife.91258.1.
11. Calderón, L. A. B., Shahidi, R. & Jékely, G. Mechanism of barotaxis in marine zooplankton. (2024) doi:10.7554/elife.94306.2.
12. Verasztó, C. *et al.* Ciliomotor circuitry underlying whole-body coordination of ciliary activity in the Platynereis larva. *Elife* **6**, (2017).

13. Ohyama, T. *et al.* A multilevel multimodal circuit enhances action selection in Drosophila. *Nature* **520**, 633–639 (2015).
14. Jovanic, T. *et al.* Competitive Disinhibition Mediates Behavioral Choice and Sequences in Drosophila. *Cell* **167**, 858–870.e19 (2016).
15. Eschbach, C. *et al.* Recurrent architecture for adaptive regulation of learning in the insect brain. *Nat Neurosci* **23**, 544–555 (2020).
16. Eschbach, C. *et al.* Circuits for integrating learned and innate valences in the insect brain. *Elife* **10**, (2021).
17. Yemini, E. *et al.* NeuroPAL: A Multicolor Atlas for Whole-Brain Neuronal Identification in C. elegans. *Cell* **184**, 272–288.e11 (2021).
18. Lin, A. *et al.* Functional imaging and quantification of multineuronal olfactory responses in. *Sci Adv* **9**, eade1249 (2023).
19. Toyoshima, Y. *et al.* Neuron ID dataset facilitates neuronal annotation for whole-brain activity imaging of C. elegans. *BMC Biol* **18**, 30 (2020).
20. Endo, Y. *et al.* Enhanced whole-brain calcium imaging and cell identification in reveal AWC neuronal responses to 2-nonanone. *J Biosci* **50**, (2025).
21. Randi, F., Sharma, A. K., Dvali, S. & Leifer, A. M. Neural signal propagation atlas of Caenorhabditis elegans. *Nature* **623**, 406–414 (2023).
22. Svara, F. *et al.* Automated synapse-level reconstruction of neural circuits in the larval zebrafish brain. *Nat Methods* **19**, 1357–1366 (2022).
23. Bock, D. D. *et al.* Network anatomy and in vivo physiology of visual cortical neurons. *Nature* **471**, 177–182 (2011).
24. Kuan, A. T. *et al.* Synaptic wiring motifs in posterior parietal cortex support decision-making. *Nature* **627**, 367–373 (2024).
25. Briggman, K. L., Helmstaedter, M. & Denk, W. Wiring specificity in the direction-selectivity circuit of the retina. *Nature* **471**, 183–188 (2011).
26. Boulanger-Weill, J. *et al.* Correlative light and electron microscopy reveals the fine circuit structure underlying evidence accumulation in larval zebrafish. *bioRxiv* (2025)

doi:10.1101/2025.03.14.643363.

27. Ahrens, M. B., Orger, M. B., Robson, D. N., Li, J. M. & Keller, P. J. Whole-brain functional imaging at cellular resolution using light-sheet microscopy. *Nat. Methods* **10**, 413–420 (2013).
28. Lemon, W. C. *et al.* Whole-central nervous system functional imaging in larval Drosophila. *Nat Commun* **6**, 7924 (2015).
29. Nguyen, J. P. *et al.* Whole-brain calcium imaging with cellular resolution in freely behaving Caenorhabditis elegans. *Proc Natl Acad Sci U S A* **113**, E1074–81 (2016).
30. Kato, S. *et al.* Global brain dynamics embed the motor command sequence of Caenorhabditis elegans. *Cell* **163**, 656–669 (2015).
31. Xu, C. S. *et al.* Enhanced FIB-SEM systems for large-volume 3D imaging. *Elife* **6**, (2017).
32. Phelps, J. S. *et al.* Reconstruction of motor control circuits in adult Drosophila using automated transmission electron microscopy. *Cell* **184**, 759–774.e18 (2021).
33. Eberle, A. L. *et al.* High-resolution, high-throughput imaging with a multibeam scanning electron microscope. *J Microsc* **259**, 114–120 (2015).
34. Vogelstein, J. T. *et al.* Discovery of brainwide neural-behavioral maps via multiscale unsupervised structure learning. *Science* **344**, 386–392 (2014).
35. Eschbach, C. & Zlatic, M. Useful road maps: studying Drosophila larva's central nervous system with the help of connectomics. *Curr Opin Neurobiol* **65**, 129–137 (2020).
36. Almeida-Carvalho, M. J. *et al.* The Ol1mpiad: concordance of behavioural faculties of stage 1 and stage 3 Drosophila larvae. *J. Exp. Biol.* **220**, 2452–2475 (2017).
37. Winding, M. *et al.* The connectome of an insect brain. *Science* **379**, eadd9330 (2023).
38. Eichler, K. *et al.* The complete connectome of a learning and memory centre in an insect brain. *Nature* **548**, 175–182 (2017).
39. Meissner, G. W. *et al.* A split-GAL4 driver line resource for Drosophila neuron types. *Elife* **13**, (2025).

40. Li, H.-H. *et al.* A GAL4 driver resource for developmental and behavioral studies on the larval CNS of Drosophila. *Cell Rep.* **8**, 897–908 (2014).
41. Thum, A. S. & Gerber, B. Connectomics and function of a memory network: the mushroom body of larval Drosophila. *Curr Opin Neurobiol* **54**, 146–154 (2019).
42. Burgos, A. *et al.* Nociceptive interneurons control modular motor pathways to promote escape behavior in. *Elife* **7**, (2018).
43. Dason, J. S. *et al.* regulates a nociceptive-like escape behavior through a developmentally plastic sensory circuit. *Proc Natl Acad Sci U S A* **117**, 23286–23291 (2020).
44. Hu, C. *et al.* Sensory integration and neuromodulatory feedback facilitate Drosophila mechanonociceptive behavior. *Nat Neurosci* **20**, 1085–1095 (2017).
45. Takagi, S. *et al.* Divergent Connectivity of Homologous Command-like Neurons Mediates Segment-Specific Touch Responses in Drosophila. *Neuron* **96**, 1373–1387.e6 (2017).
46. Dana, H. *et al.* Sensitive red protein calcium indicators for imaging neural activity. *Elife* **5**, (2016).
47. Klapoetke, N. C. *et al.* Independent optical excitation of distinct neural populations. *Nat Methods* **11**, 338–346 (2014).
48. Jenett, A. *et al.* A GAL4-driver line resource for Drosophila neurobiology. *Cell Rep* **2**, 991–1001 (2012).
49. Chen, T.-W. *et al.* Ultrasensitive fluorescent proteins for imaging neuronal activity. *Nature* **499**, 295–300 (2013).
50. Marley, R. & Baines, R. A. Whole-cell patch recording from Drosophila larval neurons. *Cold Spring Harb. Protoc.* **2011**, (2011).
51. Lemon, W. C. *et al.* Whole-central nervous system functional imaging in larval Drosophila. *Nature Communications* vol. 6 Preprint at https://doi.org/10.1038/ncomms8924 (2015).
52. Tomer, R., Khairy, K., Amat, F. & Keller, P. J. Quantitative high-speed imaging of entire

developing embryos with simultaneous multiview light-sheet microscopy. *Nat Methods* **9**, 755–763 (2012).

53. Tomer, R., Khairy, K., Amat, F. & Keller, P. J. Quantitative high-speed imaging of entire developing embryos with simultaneous multiview light-sheet microscopy. *Nat Methods* **9**, 755–763 (2012).
54. Walton, J. Lead asparate, an en bloc contrast stain particularly useful for ultrastructural enzymology. *J. Histochem. Cytochem.* **27**, 1337–1342 (1979).
55. Xu, C. S. *et al.* Enhanced FIB-SEM systems for large-volume 3D imaging. *Elife* **6**, (2017).
56. Bogovic, J. A., Hanslovsky, P., Wong, A. & Saalfeld, S. Robust registration of calcium images by learned contrast synthesis. in *2016 IEEE 13th International Symposium on Biomedical Imaging (ISBI)* (IEEE, 2016). doi:10.1109/isbi.2016.7493463.
57. Schmidt, U., Weigert, M., Broaddus, C. & Myers, G. Cell detection with star-convex polygons. in *Medical Image Computing and Computer Assisted Intervention – MICCAI 2018* 265–273 (Springer International Publishing, Cham, 2018). doi:10.1007/978-3-030-00934-2_30.
58. van der Walt, S. *et al.* scikit-image: image processing in Python. *PeerJ* **2**, e453 (2014).
59. Benjamini, Y. & Hochberg, Y. Controlling the false discovery rate: A practical and powerful approach to multiple testing. *J. R. Stat. Soc. Series B Stat. Methodol.* **57**, 289–300 (1995).
60. Saalfeld, S., Cardona, A., Hartenstein, V. & Tomancak, P. CATMAID: collaborative annotation toolkit for massive amounts of image data. *Bioinformatics* **25**, 1984–1986 (2009).
61. Winding, M. *et al.* The connectome of an insect brain. *Science* **379**, eadd9330 (2023).
62. Tracey, W. D., Jr, Wilson, R. I., Laurent, G. & Benzer, S. painless, a Drosophila gene essential for nociception. *Cell* **113**, 261–273 (2003).
63. Seligman, A. M., Wasserkrug, H. L. & Hanker, J. S. A new staining method (OTO) for enhancing contrast of lipid--containing membranes and droplets in osmium

tetroxide--fixed tissue with osmiophilic thiocarbohydrazide(TCH). *J Cell Biol* **30**, 424–432 (1966).

64. Scheffer, L. K. *et al.* A connectome and analysis of the adult Drosophila central brain. *Elife* **9**, (2020).
65. Spindler, S. R. & Hartenstein, V. The Drosophila neural lineages: a model system to study brain development and circuitry. *Dev Genes Evol* **220**, 1–10 (2010).
66. Kent, K. S., Hoskins, S. G. & Hildebrand, J. G. A novel serotonin-immunoreactive neuron in the antennal lobe of the sphinx moth Manduca sexta persists throughout postembryonic life. *J Neurobiol* **18**, 451–465 (1987).
67. Coates, K. E. *et al.* Identified Serotonergic Modulatory Neurons Have Heterogeneous Synaptic Connectivity within the Olfactory System of. *J Neurosci* **37**, 7318–7331 (2017).
68. Barsotti, E., Correia, A. & Cardona, A. Neural architectures in the light of comparative connectomics. *Curr Opin Neurobiol* **71**, 139–149 (2021).
69. Hörl, D. *et al.* BigStitcher: reconstructing high-resolution image datasets of cleared and expanded samples. *Nat Methods* **16**, 870–874 (2019).
70. Chen, F., Tillberg, P. W. & Boyden, E. S. Optical imaging. Expansion microscopy. *Science* **347**, 543–548 (2015).
71. Gallagher, B. R. & Zhao, Y. Expansion microscopy: A powerful nanoscale imaging tool for neuroscientists. *Neurobiol Dis* **154**, 105362 (2021).
72. Lillvis, J. L. *et al.* Rapid reconstruction of neural circuits using tissue expansion and light sheet microscopy. *Elife* **11**, (2022).
73. Heisenberg, M. Mushroom body memoir: from maps to models. *Nat Rev Neurosci* **4**, 266–275 (2003).
74. Dylla, K. V., Raiser, G., Galizia, C. G. & Szyszka, P. Trace Conditioning in Induces Associative Plasticity in Mushroom Body Kenyon Cells and Dopaminergic Neurons. *Front Neural Circuits* **11**, 42 (2017).
75. Campbell, R. A. A. *et al.* Imaging a population code for odor identity in the Drosophila mushroom body. *J Neurosci* **33**, 10568–10581 (2013).

76. Ganguly, I., Heckman, E. L., Litwin-Kumar, A., Clowney, E. J. & Behnia, R. Diversity of visual inputs to Kenyon cells of the Drosophila mushroom body. *Nat Commun* **15**, 5698 (2024).

77. Polizos, N. T., Dancausse, S., Rios, C. & Klein, M. Drosophila larvae form appetitive and aversive associative memory in response to thermal conditioning. *PLoS One* **19**, e0303955 (2024).

Tables

Table 1: Cell lineages that are 2-5 hops downstream of Basins and whether they were identified in the LSM whole-brain imaging dataset.

Lineage	Hop number	Responded to Basin activation
BLD2-4 L	2	yes
BLAv1/2 p L	2	yes
BLVa3/4 a L	2	yes
BLVp2 L	2	yes
CP1 v L	2	yes
CP2/3 v L	2	yes
DPLp1/2 L	2	yes
DPMm2 L	2	yes
DPMpl3 L	2	yes
BLAv1/2 a L	2	yes
BLAvm p L	2	no
BLD5/6 L	2	no
BLP3/4 b L	2	no
BLVp1 L	2	no
DPMl1 L	2	no
BLAv1/2 a L	3	yes
BLAv1/2 l L	3	yes
BLAv1/2 p L	3	yes
BLD2-4 L	3	yes
BLP1/2 a L	3	yes
BLVa3/4 a L	3	yes
BLVa3/4 t L	3	yes
BLVp1 L	3	yes
BLVp2 L	3	yes
CM1/3 L	3	yes
CM4 L	3	yes
CP1 v L	3	yes
CP2/3 d L	3	yes
CP2/3 v L	3	yes
DALv2/3 L	3	yes
DPLal1-3 L	3	yes
DPLl1-3 a L	3	yes
DPMm2 L	3	yes
DPMpl3 L	3	yes
BAla1/2 L	3	no
BAla3/4 L	3	no

BAmd1 L	3	no
BAmd2 L	3	no
BAmv1/2 L	3	no
BLAd1-4 L	3	no
BLAl L	3	no
BLAvm a L	3	no
BLAvm p L	3	no
BLD5/6 L	3	no
BLP3/4 b L	3	no
BLVa1/2 a L	3	no
CP1 d L	3	no
CP4 L	3	no
DALcl1/2 v L	3	no
DALcm1/2 m L	3	no
DALd L	3	no
DALl1 L	3	no
DALv1 L	3	no
DALv2/3 acc lat L	3	no
DALv2/3 acc med L	3	no
DALv2/3 acc ven L	3	no
DALv2/3 acc ven lat L	3	no
DPLam L	3	no
DPLc4 L	3	no
DPLc5 a L	3	no
DPLd L	3	no
DPMl1 L	3	no
DPMl2 L	3	no
DPMl3/4 p L	3	no
DPMm1 L	3	no
DPMpl1/2 L	3	no
BAlc L	4	yes
BAlp1-3 L	4	yes
BLAv1/2 a L	4	yes
BLAv1/2 l L	4	yes
BLAv1/2 p R	4	yes
BLD2-4 L	4	yes
BLP1/2 a L	4	yes
BLP1/2 b L	4	yes
BLVa3/4 a L	4	yes
BLVa3/4 b L	4	yes
BLVa3/4 t L	4	yes
BLVp1 L	4	yes

BLVp2 L	4	yes
CM1/3 L	4	yes
CM4 L	4	yes
CP1 v L	4	yes
CP2/3 d L	4	yes
CP2/3 v L	4	yes
DALv2/3 L	4	yes
DPLal1-3 L	4	yes
DPLl1-3 a L	4	yes
DPLp1/2 L	4	yes
DPMm2 L	4	yes
DPMpl3 L	4	yes
BAla1/2 L	4	no
BAla3/4 L	4	no
BAmd1 L	4	no
BAmd2 L	4	no
BAmv1/2 L	4	no
BLAd1-4 L	4	no
BLAl L	4	no
BLAv1/2 v L	4	no
BLAvm a L	4	no
BLAvm c L	4	no
BLAvm p L	4	no
BLD1 L	4	no
BLP3/4 a L	4	no
BLP3/4 b L	4	no
BLVa1/2 a L	4	no
BLVa1/2 b L	4	no
CP1 d L	4	no
CP4 L	4	no
DALcl1/2 d L	4	no
DALcl1/2 v L	4	no
DALcm1/2 m L	4	no
DALcm1/2 v L	4	no
DALd L	4	no
DALl1 L	4	no
DALv1 L	4	no
DALv2/3 acc lat L	4	no
DALv2/3 acc med L	4	no
DALv2/3 acc ven L	4	no
DALv2/3 acc ven lat L	4	no
DAMd1 L	4	no

DAMd2/3 L	4	no
DAMv1/2 L	4	no
DILP L	4	no
DPLam L	4	no
DPLc1 L	4	no
DPLc3 L	4	no
DPLc4 L	4	no
DPLc5 a L	4	no
DPLc5 p L	4	no
DPLd L	4	no
DPLl1-3 i L	4	no
DPLl1-3 L	4	no
DPLm1 L	4	no
DPLm2 L	4	no
DPMl1 L	4	no
DPMl2 L	4	no
DPMl3/4 p L	4	no
DPMm1 L	4	no
DPMpl1/2 L	4	no
DPMpm1 L	4	no
DPMpm2 L	4	no
BAlc L	5	yes
BAlp1-3 L	5	yes
BAmas1/2 L	5	yes
BLAv1/2 a L	5	yes
BLAv1/2 l R	5	yes
BLAv1/2 p L	5	yes
BLD2-4 L	5	yes
BLP1/2 a L	5	yes
BLP1/2 b L	5	yes
BLVa3/4 a L	5	yes
BLVa3/4 b L	5	yes
BLVa3/4 t L	5	yes
BLVp1 L	5	yes
BLVp2 L	5	yes
CM1/3 L	5	yes
CM4 L	5	yes
CP1 v L	5	yes
CP2/3 d L	5	yes
CP2/3 v L	5	yes
DALv2/3 L	5	yes
DPLal1-3 L	5	yes

DPLl1-3 a L	5	yes
DPLp1/2 L	5	yes
DPMm2 L	5	yes
DPMpl3 L	5	yes
KeC L	5	yes
BAla1/2 L	5	no
BAla3/4 L	5	no
BAlp4 L	5	no
BAlv L	5	no
BAmd1 L	5	no
BAmd2 L	5	no
BAmv1/2 L	5	no
BAmv3 L	5	no
BLAd1-4 L	5	no
BLAl L	5	no
BLAvm a L	5	no
BLAvm c L	5	no
BLD1 R	5	no
BLP3/4 a L	5	no
BLP3/4 b L	5	no
BLVa1/2 a L	5	no
BLVa1/2 b L	5	no
CP1 d L	5	no
DALcl1/2 v L	5	no
DALcm1/2 v L	5	no
DALd L	5	no
DALl1 L	5	no
DALv1 L	5	no
DALv2/3 acc ven L	5	no
DAMd1 L	5	no
DAMv1/2 L	5	no
DILP L	5	no
DPLam L	5	no
DPLc1 L	5	no
DPLc4 L	5	no
DPLc5 p L	5	no
DPLd L	5	no
DPLl1-3 i L	5	no
DPLm1 L	5	no
DPLm2 L	5	no
DPMl1 L	5	no
DPMl1 R	5	no

DPMl2 L	5	no
DPMl3/4 a L	5	no
DPMl3/4 p L	5	no
DPMm1 L	5	no
DPMpl1/2 L	5	no
DPMpm1 L	5	no
DPMpm2 L	5	no

Table 2: Identified brain neurons with their corresponding cell lineage and cell type. Candidate neurons, which could not be uniquely identified, are listed individually.

Left skid	Name	Cell lineage	Cell type
3044500	MB2IN-172	DPMm2	DN-SEZ
9234420	BLAv1/2 ring like	BLAv1/2	DN-SEZ
17728922	BLAv1/2 ring like	BLAv1/2	DN-SEZ
8723983	CM13 desc	CM1/3	DN-VNC
17075832	BAlp desc 1	BAlp 1-3	DN-VNC
7439913	BAlp desc 3	BAlp 1-3	DN-VNC
10915553	Switcheroo 1	CM4	DN-VNC
10609443	Switcheroo 2	CM4	DN-VNC
17732270	Switcheroo 3	CM4	DN-VNC
7227010	Switcheroo 4	CM4	DN-VNC
10945795	BLVp12 desc	BLVp2	DN-VNC
15588711	BLVp12 desc	BLVp2	DN-VNC
na	Kenyon cells	KC	KC
na	Kenyon cells	KC	KC
na	Kenyon cells	KC	KC
na	Kenyon cells	KC	KC
na	Kenyon cells	KC	KC
5118060	MB2IN-196 UT	BLAv1/2	LHNs
7910624	MBON-q1	BLAv1/2	MBON
17728723	Lasso-top 1	BAlp 1-3	na
17728730	Lasso-top 2	BAlp 1-3	na
8809171	Lasso-top 3	BAlp 1-3	na
14270761	BLVp1 bilat	BLVp1	na
5744502	PVC	BLVp2	na
6541149	BLAv12 ipsi 1	BLAv1/2	PN-somato
6623089	BLAv12 ipsi 2	BLAv1/2	pre-DN-VNC
16931001	BLAv12_ant descending 1	BLAv1/2	pre-DN-VNC
11291653	Basal-Tel-like 2	BLAv1/2	PN-somato
11263687	Basal-Tel-like 5	BLAv1/2	PN-somato
20730780	Basal-Tel-like 6	BLAv1/2	PN-somato
4966994	CM13 bilateral 3	DPMpl3	pre-DN-VNC
13849557	CSD	BALc	pre-DN-VNC